available at www.sciencedirect.com

ScienceDirect

journal homepage: www.elsevier.com/locate/chnjc

Article (Special Issue on Environmental and Energy Catalysis for Sustainable Development)

Density functional theory investigation of the enhanced adsorption mechanism and potential catalytic activity for formaldehyde degradation on Al-decorated C₂N monolayer

Yuetan Su, Wenlang Li, Guiying Li, Zhimin Ao *, Taicheng An

Guangzhou Key Laboratory of Environmental Catalysis and Pollution Control, School of Environmental Science and Engineering, Institute of Environmental Health and Pollution Control, Guangdong University of Technology, Guangzhou 510006, Guangdong, China

A R T I C L E   I N F O

A B S T R A C T

Carbonyl compounds, in particular formaldehyde (HCHO), are among the most common indoor air pollutants that have been found to be toxic to humans. Thus, in this study, density functional theory (DFT) calculations are performed to study the adsorption properties of HCHO on pristine and Al-decorated C₂N monolayer. The results indicate that Al-decorated C₂N has a strong adsorption ability for HCHO molecules with an adsorption energy of –2.585 eV. Moreover, partial density of states (PDOS), Mulliken atomic charges, and electron density distributions are calculated to investigate the adsorption enhancement mechanism. The results show that the Al atom serves as a bridge to connect the adsorbed molecules and the C₂N monolayer, thus strengthening the adsorption. Furthermore, we study the adsorption of H₂O and O₂ with the possible generation of hydroxyl (•OH) and superoxide (O₂•⁻) radicals, which are active for HCHO degradation; the results show that both molecules can also be strongly adsorbed on the Al-decorated C₂N surface. In particular, the dissociation of H₂O provides an excellent precondition for the generation of hydroxyl radicals. Our findings suggest that Al-decorated C₂N can be a promising material for the adsorption and subsequent catalytic degradation of HCHO molecules.

1. Introduction

Energy shortage and environmental pollution are two major global challenges faced by humanity today. Air pollution, which is closely related to human health, has attracted considerable attention in the past few years. Indoor air quality is particularly important for human health because humans spend 70%–90% of their life indoors [1]. Carbonyl compounds, in particular formaldehyde (HCHO), are among the most common indoor air pollutants, mainly released from decorating materials, plywood, fiberboard, particleboard, and other artificial boards [2–5]. Long-term exposure to high concentrations of HCHO may cause irritation, allergies, decreased immune function [6], and even nasopharyngeal carcinoma or leukemia [7,8]. Therefore, the removal of HCHO is a necessary measure to reduce air pollution and protect human health.

Various techniques have been reported for dealing with indoor HCHO, and the most common ones are adsorption and

catalytic oxidation. The conventional adsorption methods usually employ porous adsorbents such as activated carbon [9,10], zeolites [9,11], and molecular sieves [12], which have been widely used due to their advantages including simplicity, low cost, and room-temperature operation. However, the limited adsorption capacity and adsorbent regeneration make these systems inadequate to meet present demands [13–16]. Catalytic degradation is another widely studied process to perform HCHO oxidation [17–22]. However, it also has some shortcomings in practical applications. For example, TiO_2-based catalysts have been widely investigated, but the relatively wide band gap of TiO_2 restricts its light energy utilization; therefore, the degradation efficiency requirements are often unsatisfied [23–25]. Therefore, new catalysts for the effective removal of HCHO are still urgently needed.

Recently, a new type of carbon nitrides, the holey C_2N with two-dimensional (2D) structure, has been synthesized through a simple wet-chemical reaction [26]. As a new type of graphene-like porous structure with well-distributed pores, this material has attracted significant attention because of its ultra-large surface area and appropriate band gap value. For example, Zhu et al. [27] prepared C_2N for the adsorption of He atoms. Liu et al. [28] reported that Ca-embedded C_2N is an efficient adsorbent for CO_2 capture, while Qin et al. [29] employed charge and electric field effects to control CO_2 capture and gas separation on a C_2N monolayer. Furthermore, in the context of targeting gas pollution, Bhattachayya et al. [30] showed that a C_2N monolayer can efficiently trap HF, HCN, and H_2S pollutants, causing different changes in the *I-V* characteristics of the monolayer, which is a promising feature for the detection of the corresponding gases. These studies show that C_2N may be a promising candidate for the adsorption and degradation of HCHO molecules. However, pristine 2D materials cannot always satisfy the demands of practical applications, and functionalization is required in some cases. Previous studies have shown that modification with Al atoms can in some cases lead to enhanced adsorption capacity. For example, our previous studies have shown that Al doping of graphene can significant enhance the adsorption of CO [31] and H_2 [32,33]. In addition, Al-modified MoS_2 exhibits strong adsorption capacity toward NO_2 and NH_3 [34], while the enhanced adsorption of HCHO [35], H_2 [36], and CO_2 [37] has been observed on Al-modified BN systems. Hence, modification with Al atoms can be considered as a promising approach for improving the adsorption ability of 2D materials.

Herein, the HCHO adsorption on both pristine and Al-decorated C_2N monolayer is modeled using the density functional theory (DFT) method. Moreover, the adsorption capacity toward H_2O and O_2, which are sources of active hydroxyl and superoxide radicals, is investigated for the subsequent catalytic degradation of HCHO. Furthermore, the adsorption enhancement mechanism is analyzed by calculating the partial density of states (PDOS), Mulliken atomic charges, and electron density distribution.

2. Calculation methods

All calculations reported in this study were carried out using the DFT-based DMol[3] [38,39] module of the Materials Studio software, which includes unique methodologies and an highly efficient optimization for dealing with electrostatic problems. The Perdew-Burke-Ernzerhof (PBE) exchange-correlation functional within the generalized gradient approximation (GGA) was employed in the calculations [40]. It is essential to take into account van der Waals forces to describe the decorated metal atoms and the adsorption of gas molecules; hence, the Tkatchenko-Scheffler (TS) method for the DFT-D correction was used for this purpose. In order to take relativity effects into account, all electrons were included in the calculations, to obtain more accurate results without any special treatment of core electrons. Double numerical plus polarization (DNP) functions were adopted as the basis set. A 24 Å vacuum gap was included above the monolayer to minimize interlayer interactions. A 7×7×1 Monkhorst-Pack grid of k-points was used, and all atoms were allowed to relax until the residual forces on individual atoms were smaller than 10^{-5} Ha (1 Ha = 27.211 eV). The maximum force and displacement were set to 0.002 Ha/Å and 0.005 Å, respectively.

For examining the structural stability of Al atoms decorated on the C_2N monolayer, the binding energy $E_{b\text{-}Al}$ was determined by the relation:

$$E_{b\text{-}Al} = E_{Al+C2N} - E_{Al} - E_{C2N} \qquad (1)$$

where E_{Al+C2N}, E_{Al}, and E_{C2N} represent the total energies of the Al-decorated C_2N, an independent Al atom in the slab, and the pristine C_2N monolayer, respectively. Moreover, to probe the adsorption of gas molecules on the pristine/Al-decorated C_2N systems, the adsorption energy $E_{ad\text{-}gas}$ was determined as:

$$E_{ad\text{-}gas} = E_{C2N+gas} - E_{C2N} - E_{gas} \qquad (2)$$

where $E_{C2N+gas}$, E_{C2N}, and E_{gas} are the total energies of a gas molecule adsorbed on the C_2N layer with or without Al atoms, the isolated C_2N monolayer, and the corresponding isolated gas molecule in the slab, respectively.

3. Results and discussion

3.1. Geometrical structure of pristine and Al-decorated C_2N

The optimized structure of the C_2N monolayer unit cell is shown in Fig. 1(a), and consists of 12 C and 6 N atoms (solid black line), with four unit cells forming a uniform hole. The lattice parameters calculated in this study are $a = b$ = 8.325 Å, which are consistent with recently reported results ($a = b$ = 8.33 Å) [41,42]. Moreover, the C–N, C–C(1), and C–C(2) bond lengths are 1.337, 1.428, and 1.470 Å, respectively, also in good agreement with the recent theoretical values of 1.337, 1.429, and 1.470 Å [42]. Then, we examined the electronic properties of the pristine C_2N monolayer, whose calculated band structure is shown in Fig. 1(b). The figure shows that C_2N is a semiconductor with a direct band gap of 1.67 eV, in good agreement with the reported theoretical [43] and experimental data (1.66 and 1.96 eV, respectively) [26].

The decoration of Al atoms on the C_2N monolayer was then considered. Five different adsorption sites were examined based on the high-symmetry structure shown in Fig. 1(a). The
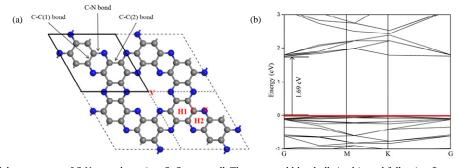
Fig. 1. (a) Top view of the structure of C$_2$N monolayer in a 2×2 supercell. The grey and blue balls in this and following figures represent the C and N atoms, respectively. A C$_2$N unit cell has been marked with a solid black line. Different adsorption sites are considered: vacancy (V), hollow-I (H1), hollow-II (H2), N-top (N) and C-top (C). (b) Band structure of pristine C$_2$N calculated by GGA-PBE.
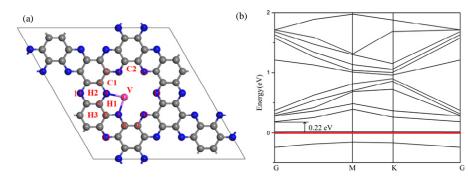

Fig. 2. (a) Top view of Al-decorated C$_2$N. The pink ball in this and following figures represents Al atom. 0–9 are the atoms besides the decorated Al atom, which are selected for Mulliken analysis. Different adsorption sites are considered: vacancy (V), hollow-Ⅰ (H1), hollow-Ⅱ (H2), hollow-Ⅲ (H3), corner-Ⅰ (C1) and corner-Ⅱ (C2). (b) Band structure of Al-decorated C$_2$N calculated by GGA-PBE.

structure of Al-decorated C$_2$N after full geometry optimization is shown in Fig. 2(a). As can be seen in the figure, the Al atom prefers to move close to the two nitrogen atoms of the C$_2$N monolayer near the vacancy (V) site, even though its initial position is on the top of a C or N atom. A similar conclusion has been reported for of Li [43] and transition metal (Pt, Co, Ni, Cu) [44] atoms decorated on a C$_2$N layer. The deposition of one Al atom on the C$_2$N monolayer causes negligible structural changes in the system, and all atoms remain in the same plane without strong deformation. In addition, the decorated Al atom forms strong chemical bonds with the two N atoms, with a bond length of 1.97 Å. It should be noted that this bond length is longer than both the C–C and C–N bonds in the C$_2$N monolayer, which reveals that the Al–N bonds are easily broken in a chemical reaction, compared with the pristine C$_2$N system. Previous research has shown that a high concentration of metal atoms leads to their aggregation; in order to verify the structural stability of the Al-decorated C$_2$N system, the binding energy (E_b) was calculated based on Eq. (1). Table S1 (Supporting Information) shows the calculated binding energy of the decorated Al atom at different positions on the pristine C$_2$N monolayer. The results show that the V site has the highest binding energy (E_b = −4.57 eV), which exceeds the cohesive energy of bulk Al (−3.39 eV/atom) [45]. Thus, the aggregation of Al atoms in the C$_2$N monolayer can be neglected, confirming the stability of Al-decorated C$_2$N. It is worth mentioning that the decorated Al atom leads to a sharp decrease in the band gap from 1.69 to 0.22 eV, as shown in Fig. 2(b), and a similar phenomenon has

been also reported by Hashmi et al. [43] for a Li-decorated C$_2$N monolayer. A 3×3 C$_2$N supercell was constructed to assess the effect of the loading amount of Al on the adsorption of both Al atoms and HCHO molecules. After geometry optimization, the structures of the 3×3 Al-decorated C$_2$N monolayer with and without adsorbed HCHO are shown in Fig. S1. Compared with the 2×2 C$_2$N monolayer supercell (Al loading amount ~2.9 wt%), the calculated binding energy of the Al atom on the 3×3 C$_2$N monolayer supercell (Al loading amount ~1.3 wt%) slightly increases to −4.87 eV. In addition, the adsorption energy of the HCHO molecule on the Al-decorated C$_2$N also shows a slight change, to −2.33 eV. Therefore, the Al loading amount has a negligible effect on the HCHO adsorption; the maximum Al loading amount can reach ~10.6 wt% with one Al atom at each hollow site of the C$_2$N monolayer. Higher Al loadings were also considered, with two or three Al atoms decorated on the same hollow site; however, Al aggregation occurs in these cases, which would negatively affect the adsorption of HCHO molecules and also the possible catalytic degradation performance.

To further understand the strong binding between the decorated Al atom and the C$_2$N monolayer, we carried out an electron population analysis using the Mulliken method. Because the decorated Al atom mainly affects the charge distribution in the nearby region, to better describe the electron variation we analyzed the atomic charges of the Al atom and of 14 atoms (sites 1–14 in Fig. 2) close to it. The results are listed in Table 1. As shown in the table, the electrons show good dispersion on the pristine C$_2$N monolayer, where the C atoms have charges of

Table 1

Atomic charges of pristine/Al-decorated C_2N monolayer calculated by Mulliken analysis. The unit of the charge is one electron charge e.

Atom number	Intrinsic C_2N	Al-decorated C_2N
0(Al)	—	0.843
1(N)	−0.270	−0.414
2(C)	0.135	0.152
3(C)	0.133	0.217
4(N)	−0.267	−0.630
5(C)	0.135	0.233
6(C)	0.136	0.234
7(N)	−0.268	−0.616
8(C)	0.133	0.232
9(C)	0.133	0.160
10(N)	−0.270	−0.410
11(N)	−0.267	−0.318
12(N)	−0.268	−0.314
13(N)	−0.268	−0.272
14(N)	−0.267	−0.270

0.133–0.135 e, whereas the charges of the N atoms vary between −0.267 and −0.270 e. After decorating an Al atom, the electron distribution shows a marked variation. The Al atom transfers electrons to the atoms near the vacancy, and carries a +0.843 e charge. In particular, for the N atoms at sites 4 and 7, which are directly connected with the Al atom, the electronic charges change from −0.267 and −0.268 e to −0.630 and −0.616 e, respectively. For the N atoms close to the vacancy at sites 1, 10, 11, and 12, the charges are −0.414, −0.410, −0.318, and −0.314 e, respectively, showing a decreasing ability to attract electrons, which also reflects the distances between the N atoms and the Al atom. The N atoms at sites 13 and 14, close to another vacancy, have electronic charges of −0.270 and −0.272 e, respectively, similar to those in the pristine C_2N system. This indicates that the decorated Al atom mainly affects the electron distribution close to the vacancy, and a large number of electrons transfer from the Al atom, leading to a strong binding between the Al atom and the C_2N layer, as well as achieving a high stability of the decorated structure.

Table 2

Results of favorite adsorption configurations of HCHO, H_2O and O_2 adsorbed on intrinsic/Al-decorated C_2N monolayer, respectively. $E_{\text{ad-gas}}$ and d are adsorption energies and adsorption distances between gas molecules and C_2N monolayer. l is the bond lengths of decorated Al atom and the adsorbed gas molecules.

Type	Intrinsic C_2N		Al-decorated C_2N		
	$E_{\text{ad-gas}}$ (eV)	d (Å)	$E_{\text{ad-gas}}$ (eV)	l (Å)	d (Å)
HCHO	−0.583	1.132	−2.586	1.706	1.382
H_2O	−0.743	0.986	−3.177	1.709	—
O_2	−0.206	1.455	−2.767	1.791/1.765	1.789

3.2. Adsorption behavior of HCHO molecules

The adsorption of HCHO molecules on the C_2N monolayer was then investigated. Based on the high-symmetry structure, five possible adsorption sites were investigated, denoted as V, C, N, H1, and H2 in Fig. 1(a). After structural relaxation, the most stable adsorption configuration is observed at the V site, with an adsorption energy $E_{\text{ad-gas}}$ of −0.583 eV, calculated from Eq. (2). The structure of this configuration is shown in Fig. 3(a), and the corresponding structural parameters are listed in Table 2. The figure shows that the HCHO molecule prefers to sit on the vacancy site, with the oxygen atom up and the two hydrogen atoms pointing down; the molecule is located 1.132 Å away from the C_2N monolayer and the adsorption energy is −0.583 eV. This short distance is in the range of chemical bonds; however, as can be seen in the figure, the adsorbed HCHO molecule is embedded in the vacancy site of C_2N, and no chemical bonds are formed. In addition, the adsorption causes negligible structural changes in both the HCHO molecule and C_2N layer, denoting a physisorption behavior. After adsorption, the C–O and C–H lengths in the HCHO molecule change from 1.212 and 1.117 Å to 1.218 and 1.113 Å, respectively. All atoms in the C_2N layer maintain a flat arrangement. Table S2 shows the calculated adsorption energies at different adsorption sites, which further confirm that the HCHO molecule adsorbed on the pris-
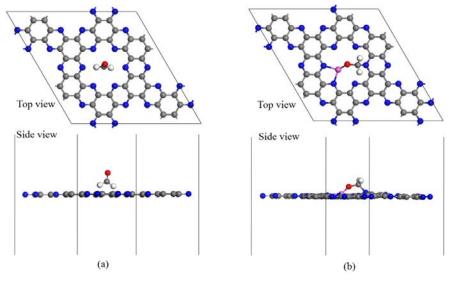

Fig. 3. The favorite adsorption configurations of a HCHO molecule adsorbed on (a) intrinsic C_2N monolayer and (b) Al-decorated C_2N monolayer. The red and white balls in this and following figures represent the O and H atoms, respectively.

tine C_2N monolayer undergoes weak physisorption.

Then, we investigated the adsorption of the HCHO molecule on the Al-decorated C_2N monolayer, focusing on six possible sites (V, H1, H2, H3, C1, and C2) besides the decorated Al atom, as shown in Fig. 2(a). The corresponding calculated adsorption energies at these six sites are listed in Table S3. The results show that the preferred adsorption structure involves the HCHO molecule lying on the V site, with an adsorption energy of –2.585 eV, as shown in Fig. 3(b). The figure shows the presence of two chemical bonds (Al–O and C–N) between the HCHO molecule and the C_2N layer, and the corresponding bond lengths are 1.706 Å (Al–O bond) and 1.524 Å (C–H bond), respectively. As also shown in the figure, the strong adsorption causes the structural distortion of the C_2N layer, which exhibits a slight curvature. In particular, the Al and N atoms connected with the adsorbed HCHO molecule move toward it, attracting its C atom toward the C_2N layer. The C–O and C–H bond lengths of the HCHO molecule change from 1.212 and 1.117 Å to 1.383 and 1.100 Å, respectively, exhibiting a different adsorption behavior compared with the pristine system. It is worth mentioning that the Al-decorated C_2N monolayer shows a better performance for HCHO adsorption compared with that previously reported for Fe-doped graphene ($E_{ad\text{-}gas}$ = –1.45 eV) [46] and Ti-doped graphene ($E_{ad\text{-}gas}$ = –2.26 eV) [47], revealing the potential application for HCHO concentration, use, and treatment.

To further understand the mechanism behind the enhanced adsorption of HCHO molecules on the Al-decorated C_2N, the PDOS plots of HCHO and pristine/Al-decorated C_2N were calculated and displayed in Fig. 4. The overlap between bands in the PDOS is representative of the adsorption strength. For ad-

Table 3
Atomic charges of the absorbed molecules in pristine/Al-derocated C_2N monolayer calculated by Mulliken analysis. The unit of charge is *e*.

Type	Intrinsic C_2N	Al-decorated C_2N	
	Adsorbed molecule	Al atom	Adsorbed molecule
HCHO	0.115	–0.228	1.207
H_2O	0.065	–0.349	1.159
O_2	0.037	–0.654	1.243

sorption on the Al-decorated C_2N monolayer, electron interactions can be clearly observed between the adsorbed molecule, the decorated Al atom, and the C_2N monolayer, as indicated by the blue dashed area in Fig. 4(b). However, in the pristine system, these interactions only involve the adsorbed molecule and the C_2N monolayer, as indicated by the red dashed area. In other words, in the Al-decorated system, the electrons of the adsorbed molecule interact not only with the electrons in the C_2N monolayer, but also with those of the decorated Al atom. Thus, the Al atom acts as a bridge connecting the HCHO molecule and the C_2N monolayer, which strengthens the interaction between electrons and enhances the adsorption. In addition, the PDOS curve of the Al-decorated system is shifted to the left (i.e., toward lower energies) compared to that of the pristine system, indicating a more stable adsorption.

Furthermore, the Mulliken population analysis was performed to obtain the specific charges of the HCHO molecule and Al atoms. The results are displayed in Table 3. A considerably stronger electron transfer is observed in the Al-decorated system, indicating a stronger interaction between the HCHO molecule and the C_2N layer. To analyze the distribution of electrons in more detail, we calculated the electron density distribution
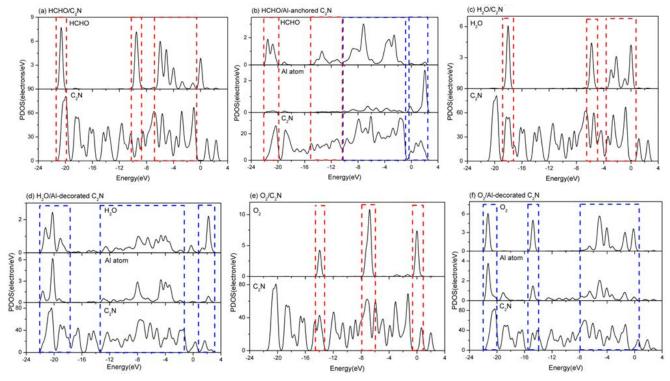

Fig. 4. The PDOS of adsorbed gas molecules, decorated Al atom and C_2N monolayer. The red dash indicates the overlap areas of adsorbed molecules and C_2N, while the blue dash indicates the overlap areas of the adsorbed molecules, the decorated Al atom and the C_2N.
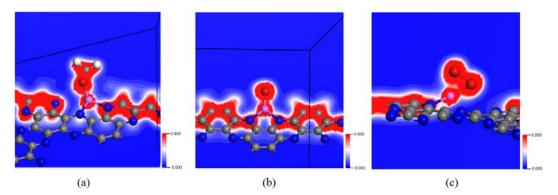
Fig. 5. Electronic density distribution of (a) HCHO, (b) H_2O, and (c) O_2 adsorbed on the Al-decorated C_2N.

of the HCHO molecule adsorbed on Al-decorated C_2N, shown in Fig. 5(a). The electron cloud extends over the decorated Al atom, the C_2N monolayer, and the adsorbed HCHO molecule, which is consistent with the band overlap in the PDOS shown in Fig. 4(a), and induces the strong adsorption of gas molecules. In addition, a relatively higher density of the electron cloud can be observed among the decorated Al atom, the C_2N monolayer, and the adsorbed HCHO molecule. These results further confirm that the Al atom acts as a bridge connecting the HCHO molecule and the C_2N layer. This indicates that the decorated Al atom alters the electron distribution and lead to the enhanced adsorption of HCHO molecules, which is in good agreement with the other results discussed above.

3.3. Adsorption of H_2O and O_2 molecules for possible catalytic degradation of HCHO

As discussed above, the HCHO molecule can be strongly adsorbed on the Al-decorated C_2N, which provides an excellent precondition for the subsequent treatment. Different techniques for the degradation of HCHO molecules are available, such as electro-Fenton [48], electro-oxidation [49,50], and photocatalysis processes [51–53]. Among these degradation methods, the generation of the hydroxyl (•OH) and superoxide ($O_2^{•-}$) radicals usually plays a crucial role in the oxidation pro-

cesses [54–61]. As these two radicals are generally derived from H_2O and O_2, it is also necessary to investigate the adsorption behavior of these two molecules. Therefore, we also investigated the adsorption of H_2O and O_2 molecules on pristine and Al-decorated C_2N monolayer. Similar to the adsorption of volatile organic compounds (VOCs) discussed above, we considered five possible adsorption sites (V, C, N, H1, and H2 as shown in Fig. 1(a)) on the pristine C_2N monolayer and six possible sites (V, H1, H2, H3, C1, and C2 as shown in Fig. 2(a)), besides the decorated Al atom, on the Al-decorated C_2N monolayer. The calculated adsorption energies are listed in Table S2 and Table S3, respectively.

The most stable configurations for a water molecule adsorbed on the pristine and Al-decorated C_2N monolayer are shown in Figs. 6(a) and 6(b), respectively, and the corresponding structural parameters are listed in Table 2. In the pristine system, Fig. 6(a) shows that the H_2O molecule prefers to lie above the V site of the C_2N monolayer, with the oxygen atom up and the two hydrogen atoms pointing downward. The calculated adsorption energy is –0.743 eV. The distance between the H_2O molecule and the C_2N monolayer is 0.986 Å, and no chemical bonds are formed. The two O–H bond lengths of the water molecule increase from 0.968 Å in the isolated H_2O molecule to 0.978 Å in the adsorbed state. After Al atom decoration on the C_2N layer, the most stable adsorption configuration is shown in
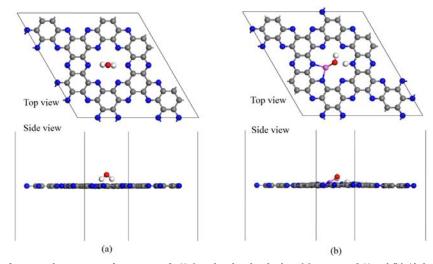

Fig. 6. The favorite adsorption configurations of a H_2O molecule adsorbed on (a) intrinsic C_2N and (b) Al-decorated C_2N.
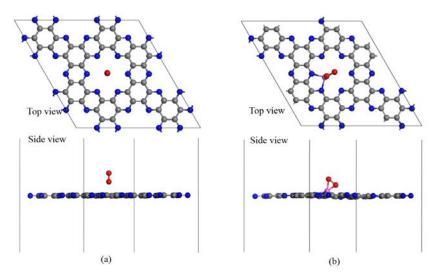
Fig. 7. The favorite adsorption configurations of an O_2 molecule adsorbed on (a) intrinsic C_2N and (b) Al-decorated C_2N.

Fig. 6(b). The obtained adsorption energy is −3.177 eV, which is around four times higher than that measured in the pristine system. This strong adsorption causes slight structural changes in the Al-decorated C_2N sheet as well as induces the dissociation of the H_2O molecule into an −OH group and a H atom, which is attached to the decorated Al atom with Al−O and N−H bond lengths of 1.709 and 1.049 Å, respectively. This indicates a very strong interaction between the H_2O molecule and the Al-decorated C_2N.

In the case of O_2 adsorption on pristine and Al-decorated C_2N monolayer, we found that the O_2 molecule also prefers to adsorb on the V site; the most stable structure is shown in Fig. 7(a). As shown in the figure, in the pristine C_2N system the O_2 molecule lies perpendicular to the center of the vacancy site, with an adsorption energy of −0.206 eV. This relatively weak adsorption has negligible impact of the C_2N monolayer. The O−O bond length of the O_2 molecule increases from 1.225 Å in an isolated O_2 molecule to 1.288 Å after adsorption. In addition, the O_2 molecule is nearly 1.5 Å away from the C_2N layer, which is large than the distance observed for the HCHO molecule (around 0.9 Å), and the corresponding adsorption energy is also lower than that of the HCHO molecule (−0.743 eV). However, in the Al-decorated system, regardless of its initial position, the O_2 molecule prefers to move to the V site after geometry optimization; the final structure is shown in Fig. 7(b). The O_2 molecule prefers to lie near the vacancy site (E_{ad-gas} = −2.767 eV); as the O=O bond breaks, both O atoms form chemical bonds with the Al atom, as shown in the side view of Fig. 5(b). The two Al−O bond lengths are 1.791 and 1.765 Å, while the O−O bond length increases to 1.516 Å, which is much longer than that of an isolated O_2 molecule (1.225 Å) and of the O_2 molecule adsorbed on the pristine C_2N monolayer (1.288 Å). Furthermore, the Al-decorated C_2N monolayer exhibits slight distortion with the Al atom shifted toward the adsorbed O_2 molecule.

Therefore, the decoration of Al atoms on C_2N can significantly enhance the adsorption of H_2O and O_2 molecules as well. In particular, the hydroxyl group can be formed directly upon H_2O adsorption, which greatly benefits the generation of hydroxyl radicals. On the other hand, the chemisorbed O_2 molecules also have a much higher ability to attract additional electrons, with a high potential to be activated into superoxide radicals. Therefore, the Al-decorated C_2N could be a promising novel material for concentrating VOCs, as well as for their degradation through radical routes.

Similar to the case of HCHO molecules on the Al-decorated C_2N monolayer, the PDOS of the H_2O and O_2 molecules on the pristine/Al-decorated C_2N systems were also calculated and are displayed in Fig. 4. Based on the band overlap, the electron interactions between the H_2O or O_2 molecule, the decorated Al atom, and the C_2N monolayer (indicated as blue dashed areas in Figs. 6(d) and 6(f)) are considerably stronger than the interaction in the pristine system, indicated by the red dashed band overlap in Figs. 6(c) and 6(e). Therefore, a similar adsorption enhancement mechanism can be achieved, with the Al atom acting as a bridge to connect the H_2O or O_2 molecule and the C_2N monolayer, strengthening the interaction between electrons and enhancing the adsorption. In addition, Mulliken atomic charges were calculated for the H_2O and O_2 molecules on the pristine and Al-decorated C_2N systems, and the results are listed in Table 3, while the corresponding electron density distribution is shown in Figs. 5(b) and 5(c). Similar to HCHO, the electron transfer is considerably stronger in the Al-decorated system, and the electron cloud extends over the adsorbed HCHO, the decorated Al atom, and the C_2N monolayer, inducing the strong adsorption of the gas molecules.

4. Conclusions

The adsorption behavior of the HCHO molecule and the potential catalytic degradation ability of pristine and Al-decorated C_2N monolayer were investigated using first-principles calculations. Because the adsorption of the HCHO molecule on the pristine C_2N monolayer is relatively weak (E_{ad-gas} = −0.583 eV) and not suitable for its concentration and subsequent treatment, Al atoms were decorated on the C_2N layer, resulting in a

high HCHO adsorption energy of –2.586 eV. Moreover, the H_2O and O_2 molecules were strongly adsorbed on the Al-decorated C_2N monolayer, providing a favorable precondition for the possible generation of hydroxyl and superoxide radicals. In particular, the H_2O molecule dissociated spontaneously and generated a hydroxyl group connected with the Al atom on the C_2N surface, revealing its promising potential for the generation of hydroxyl radicals. Furthermore, we investigated the adsorption enhancement mechanism for HCHO, H_2O, and O_2 molecules. The results showed that the decorated Al atom can alter the electron distribution and thus the chemical and physical properties in its vicinity, acting as a bridge between the HCHO molecule and the C_2N layer, and strengthening the adsorption. Hence, the Al-decorated C_2N monolayer proved to be an excellent material for the adsorption and possible catalytic degradation of HCHO molecules.

References

[1] N. E. Klepeis, W. C. Nelson, W. R. Ott, J. P. Robinson, A. M. Tsang, P. Switzer, J. V. Behar, S. C. Hern, W. H. Engelmann, *J. Expo. Anal. Environ. Epidemiol.*, **2001**, 11, 231–252.

[2] T. Salthammer, S. Mentese, R. Marutzky, *Chem. Rev.*, **2010**, 110, 2536–2572.

[3] R. K. Nath, M. F. M. Zain, M. Jamil, *Renew. Sustain. Energy Rev.*, **2016**, 62, 1184–1194.

[4] U. Schlink, S. Röder, T. Kohajda, D. K. Wissenbach, U. Franck, I. Lehmann, *Build. Environ.*, **2016**, 105, 198–209.

[5] Y. Su, Z. Ao, Y. Ji, G. Li, T. An, *Appl. Surf. Sci.*, **2018**, 450, 484–491.

[6] K. A. Mundt, A. E. Gallagher, L. D. Dell, E. A. Natelson, P. Boffetta, P. R. Gentry, *Crit. Rev. Toxicol.*, **2017**, 47, 598–608.

[7] M. Hauptmann, J. H. Lubin, P. A. Stewart, R. B. Hayes, A. Blair, *Am. J. Epidemiol.*, **2004**, 159, 1117–1130.

[8] X. Tang, Y. Bai, A. Duong, M. T. Smith, L. Li, L. Zhang, *Environ. Int.*, **2009**, 35, 1210–1224.

[9] X. S. Zhao, Q. Ma, G. Q. Lu, *Energy Fuels*, **1998**, 12, 1051–1054.

[10] J. Li, P. Zhang, J. Wang, M. Wang, *J. Phys. Chem. C*, **2016**, 120, 24121–24129.

[11] J. H. Shen, Y. S. Wang, J. P. Lin, S. H. Wu, J. J. Horng, *J. Air Waste Manage. Assoc.*, **2014**, 64, 13–18.

[12] X. Zhu, J. Yu, C. Jiang, B. Cheng, *Phys. Chem. Chem. Phys.*, **2017**, 19, 6957–6963.

[13] L. Nie, J. Yu, M. Jaroniec, F. F. Tao, *Catal. Sci. Technol.*, **2016**, 6, 3649–3669.

[14] R. R. Bansode, J. N. Losso, W. E. Marshall, R. M. Rao, R. J. Portier, *Bioresource Technol.*, **2003**, 90, 175–184.

[15] V. Boonamnuayvitaya, S. Sae-ung, W. Tanthapanichakoon, *Sep. Purif. Technol.*, **2005**, 42, 159–168.

[16] Y. Matsuo, Y. Nishino, T. Fukutsuka, Y. Sugie, *Carbon*, **2008**, 46, 1162–1163.

[17] T. Liu, F. Li, X. Li, *J. Hazard. Mater.*, **2008**, 152, 347–355.

[18] A. A. Ismail, *Appl. Catal. B*, **2012**, 117–118, 67–72.

[19] Z. Xu, J. Yu, W. Xiao, *Chem. Eur. J.*, **2013**, 19, 9592–9598.

[20] R. J. Wu, Y. S. Liu, H. F. Lai, J. H. Wang, M. Chavali, *J. Nanosci. Nanotechnol.*, **2014**, 14, 6792–6799.

[21] I. Jansson, S. Suárez, F. J. Garcia–Garcia, B. Sánchez, *Appl. Catal. B*, **2015**, 178, 100–107.

[22] B. Bai, Q. Qiao, J. Li, J. Hao, *Chin. J. Catal.*, **2016**, 37, 102–122.

[23] R. Liu, J. Wang, J. Zhang, S. Xie, X. Wang, Z. Ji, *Microporous Mesoporous Mater.*, **2017**, 248, 234–245.

[24] J. Melcher, S. Feroz, D. Bahnemann, *J. Mater. Sci.*, **2017**, 52, 6341–6348.

[25] J. Shang, W. W. Xu, C. X. Ye, C. George, T. Zhu, *Sci. Rep.*, **2017**, 7, 1161/1–1161/9.

[26] J. Mahmood, E. K. Lee, M. Jung, D. Shin, I. Y. Jeon, S. M. Jung, H. J. Choi, J. M. Seo, S. Y. Bae, S. D. Sohn, N. Park, J. H. Oh, H. J. Shin, J. B. Baek, *Nat. Commun.*, **2015**, 6, 6486.

[27] L. Zhu, Q. Xue, X. Li, T. Wu, Y. Jin, W. Xing, *J. Mater. Chem. A*, **2015**, 3, 21351–21356.

[28] Y. Liu, Z. Meng, X. Guo, G. Xu, D. Rao, Y. Wang, K. Deng, R. Lu, *Phys. Chem. Chem. Phys.*, **2017**, 19, 28323–28329.

[29] G. Q. Qin, A. J. Du, Q. Sun, *Energy Technol.*, **2018**, 6, 205–212.

[30] K. Bhattacharyya, S. M. Pratik, A. Datta, *J. Phys. Chem. C*, **2018**, 122, 2248–2258.

[31] Z. M. Ao, J. Yang, S. Li, Q. Jiang, *Chem. Phys. Lett.*, **2008**, 461, 276–279.

[32] Z. M. Ao, Q. Jiang, R. Q. Zhang, T. T. Tan, S. Li, *J. Appl. Phys.*, **2009**, 105, 074307/1–074307/6.

[33] Z. M. Ao, F. M. Peeters, *Phys. Rev. B*, **2010**, 81, 205406/1–205406/7.

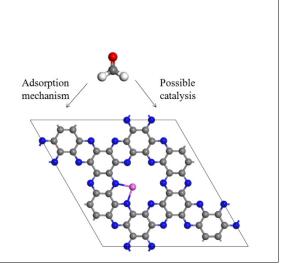[34] H. Luo, Y. Cao, J. Zhou, J. Feng, J. Cao, H. Guo, *Chem. Phys. Lett.*,

---

Graphical Abstract

Density functional theory investigation of the enhanced adsorption mechanism and potential catalytic activity for formaldehyde degradation on Al-decorated C_2N monolayer

Yuetan Su, Wenlang Li, Guiying Li, Zhimin Ao *, Taicheng An
Guangdong University of Technology

Al-decorated C_2N can enhance the HCHO adsorption capacity and the subsequent generation of hydroxyl (•OH) and superoxide ($O_2^{•-}$) radicals; therefore, it represents a promising material for the adsorption and possible catalytic degradation of HCHO.

2016, 643, 27–33.

[35] S. Noorizadeh, E. Shakerzadeh, *Comput. Mater. Sci.*, **2012**, 56, 122–130.

[36] S. Q. Ma, *Adv. Mater. Res.*, **2011**, 197–198, 701–704.

[37] P. Shao, X. Y. Kuang, L. P. Ding, J. Yang, M. M. Zhong, *Appl. Surf. Sci.*, **2013**, 285, 350–356.

[38] B. Delley, *J. Chem. Phys.*, **1990**, 92, 508–517.

[39] B. Delley, *J. Chem. Phys.*, **2000**, 113, 7756–7764.

[40] J. P. Perdew, K. Burke, M. Ernzerhof, *Phys. Rev. Lett.*, **1998**, 80, 891.

[41] Y. Yang, M. Guo, G. Zhang, W. Li, *Carbon*, **2017**, 117, 120–125.

[42] S. Guan, Y. Cheng, C. Liu, J. Han, Y. Lu, S. A. Yang, Y. Yao, *Appl. Phys. Lett.*, **2015**, 107, 231904/1–231904/5.

[43] A. Hashmi, M. U. Farooq, I. Khan, J. Son, J. Hong, *J. Mater. Chem. A*, **2017**, 5, 2821–2828.

[44] X. Li, W. Zhong, P. Cui, J. Li, J. Jiang, *J. Phys. Chem. Lett.*, **2016**, 7, 1750–1755.

[45] R. Gaudoin, W. M. C. Foulkes, G. Rajagopal, *J. Phys. Condens. Mat.*, **2002**, 14, 8787–8793.

[46] D. Cortés–Arriagada, N. Villegas-Escobar, S. Miranda-Rojas, A. Toro–Labbé, *Phys. Chem. Chem. Phys.*, **2017**, 19, 4179–4189.

[47] H. P. Zhang, X. G. Luo, X. Y. Lin, X. Lu, Y. Leng, H. T. Song, *Appl. Surf. Sci.*, **2013**, 283, 559–565.

[48] G. Moussavi, A. Bagheri, A. Khavanin, *J. Hazard. Mater.*, **2012**, 237–238, 147–152.

[49] S. N. Azizi, S. Ghasemi, M. Derakhshani-mansoorkuhi, *Int. J. Hydrogen Energy*, **2016**, 41, 21181–21192.

[50] Y. Huang, K. Ye, H. Li, W. Fan, F. Zhao, Y. Zhang, H. Ji, *Nano Res.*, **2016**, 9, 3881–3892.

[51] G. Wu, C. Zhao, C. Guo, J. Chen, Y. Zhang, Y. Li, *Appl. Surf. Sci.*, **2018**, 428, 954–963.

[52] Z. Shayegan, C. S. Lee, F. Haghighat, *Chem. Eng. J.*, **2018**, 334, 2408–2439.

[53] G. Zhang, A. Song, Y. Duan, S. Zheng, *Microporous Mesoporous Mater.*, **2018**, 255, 61–68.

[54] G. Mamba, A. K. Mishra, *Appl. Catal. B*, **2016**, 198, 347–377.

[55] B. Jing, Z. Ao, Z. Teng, C. Wang, J. Yi, T. An, *Sustain. Mater. Technol.*, **2018**, 16, 12–22.

[56] J. Li, P. Yan, K. Li, W. Cen, X. Yu, S. Yuan, Y. Chu, Z. Wang, *Chin. J. Catal.*, **2018**, 39, 1695–1703.

[57] J. Li, X. Dong, Y. Sun, G. Jiang, Y. Chu, S. C. Lee, F. Dong, *Appl. Catal. B*, **2018**, 239, 187–195.

[58] T. Liao, Z. Sun, J. H. Kim, S. X. Dou, *Nano Energy*, **2017**, 32, 209–215.

[59] T. Liao, L. Kou, A. Du, Y. Gu, Z. Sun, *J. Am. Chem. Soc.*, **2018**, 140, 9159–9166.

[60] T. Liao, Z. Sun, C. Sun, S. X. Dou, D. J. Searles, *Sci. Rep.*, **2014**, 4, 6256/1–6256/7.

[61] T. Liao, L. Kou, A. Du, L. Chen, C. Cao, Z. Sun, *Adv. Theory Simul.*, **2018**, 1, 1700033.

Al修饰C₂N对甲醛降解的吸附增强机理及潜在催化活性的密度泛函理论研究

苏岳檀，李文浪，李桂英，敖志敏*，安太成

广东工业大学环境健康与污染控制研究院，环境科学与工程学院，广州市环境催化及污染控制重点实验室，广东广州510006

摘要: 羰基化合物, 特别是甲醛, 是室内最常见的对人体有害的空气污染物之一. 如何对甲醛进行有效的控制已成为当前研究热点. 在本工作中, 我们使用密度泛函理论化学计算方法研究了甲醛分子在C₂N和Al修饰C₂N上的吸附性能. 结果表明, 纯C₂N对甲醛分子的吸附能力较弱, 吸附能仅为–0.583 eV, C₂N经Al原子修饰改性后, 吸附能为–2.585 eV, 超过了改性前的4倍, 有效增强了体系对甲醛分子的吸附能力. 为了研究甲醛分子在Al修饰C₂N上的吸附增强机理, 我们对局部态密度 (PDOS)、Mulliken电荷分布及电子密度分布进行了计算. 结果表明, Al原子修饰改变了附近的电子分布, 从而改变了修饰Al原子的化学和物理行为, 使其起到了连接甲醛分子和C₂N层的桥梁作用, 从而加强了吸附能力.

此外, 为了研究产生对甲醛活化有效的羟基自由基(•OH)和超氧(O₂⁻)自由基的可能, 我们还计算了C₂N结构对H₂O分子和O₂分子的吸附. 结果表明, Al修饰的C₂N对H₂O分子和O₂分子同样有很强的吸附能力. 对于H₂O分子, 在纯C₂N结构中的吸附能为–0.743 eV, 在Al原子修饰后的结构中, 其吸附能高达–3.177 eV, 并且此时H₂O分子能够自发解离成一个羟基和一个H原子, 其中羟基与修饰的Al原子相连, 这为羟基自由基的生成提供了良好的条件. 而对于O₂分子, 在纯C₂N结构中的吸附能仅为–0.206 eV, 在Al原子修饰后其吸附能高达–2.767 eV, 约为修饰前的13倍, 这使得化学吸附的O₂分子也具有更高的获得额外电子和高电位被激活为超氧自由基的潜能, 这也为超氧自由基的生成提供了良好基础. 上述研究表明, Al修饰C₂N是一种有前途的材料, 可用于甲醛分子的吸附及催化降解.

关键词: C₂N; 密度泛函理论; 二维材料; 甲醛; 吸附; 催化降解